Desalination and Water Treatment
www.deswater.com

doi: 10.5004/dwt.2019.24754

171 (2019) 132–143
December

Improvement of the performance of PES nanocomposite membrane incorporated with citric acid-modified graphene oxide for the removal of heavy metals

Masoumeh Arash, Yaghoub Mansourpanah*, Ali Kakanejadifard

Membrane Research Laboratory, Lorestan University, 68137-17133 Khorramabad, Iran, Tel./Fax: +98 66 33120618;
emails: mansourpanah.y@lu.ac.ir (Y. Mansourpanah), m.arash2000@yahoo.com (M. Arash), kakanejadi.a@lu.ac.ir (A. Kakanejadifard)

Received 9 February 2019; Accepted 31 July 2019

ABSTRACT

This work reports the preparation of a high performance polyethersulfone mixed matrix nanocomposite membrane incorporated with citric acid-decorated graphene oxide (GO-CA). The effect of the additive on morphology, performance and antifouling properties of the prepared membranes was investigated using common available techniques. Scanning electron microscopy images illustrated no cracks on the top of the surface, showing favorable dispersing of GO-CA in the bulk of the modified membranes. In addition, the retention ability of the membranes towards Cr^{3+} and Pb^{2+} ions was increased to over four times at appropriate dosages of GO-CA. In this regard, the mixed matrix membranes composed of GO-CA nanosheets showed a remarkable and desired antifouling properties (over 99.4% in comparison with 86.2% for the pristine membrane) during filtration of bovine serum albumin solution. The results clearly indicated that the alteration of roughness and hydrophilicity causes the suppression of fouling owing to the presence of GO-CA. Eventually, the alteration in surface charge (Donnan exclusion) and pore size (steric hindrance) of the membranes composed of GO-CA determined the value of rejection.

Keywords: Graphene oxide-citric acid; Polyethersulfone membrane; Heavy metal retention; Low fouling; Donnan exclusion

1. Introduction

In recent years, water resources have been polluted by heavy metal ions owing to population growth, industrial development and reduced water supply due to reduced rainfall. Heavy metals have high toxicity and are environmentally stable. They can pollute soil and water and have a tendency to accumulate in body tissues. Common techniques that are used for the treatment of heavy metals in water include chemical precipitation, membrane processes, ion exchange and adsorption. Advantages of the membrane process compared to other methods in the separation of heavy metals are lack of phase changing, energy saving, high separation efficiency, easy scale up and environmentally friendliness. In the past decade, application of nanofiltration membranes (NF) for the removal of heavy metals has attracted great attention due to their high water permeability, low operation pressure and low energy consumption. Due to its high tensile strength, chemical stability against aggressive media, and desired Tg of about 220°C, polyethersulfone (PES) is a suitable polymer for the preparation of NF membranes [1]. Many researchers have relied on nanotechnology and nanomaterials for improving the performance of PES membranes. Among differing nanomaterial, graphene oxide (GO) have attracted great attention due to its remarkable thermal, mechanical and electronic properties [2]. Many functional groups, such as −COOH, −C=O and −OH, can be introduced on GO surface by the oxidization of GO. These functional groups are necessary for adsorbing metal ions.

Meng et al. [2] evaluated the effect of trace GO in coagulation bath on the morphology of polysulfone (PS) membranes. Although, the hydrophilicity of PS/GO membranes enhanced, the salt rejection and pure water flux of the modified membranes became slightly lower than unmodified membranes. Zinadini et al. [1] evaluated the effect of GO on PES matrix

* Corresponding author.

membranes which they showed a desired enhancement in pure water flux, salt rejection, mean pore radius, porosity and antifouling ability of the modified membranes.

In order to improve the performance of GO in heavy metal removal, GO can be functionalized by citric acid (CA). In the meantime, our goal was to study the synthesis and application of CA-modified GO to fabricate PES-based mixed matrix membrane for the evaluation of synergistic influence of CA and GO on the properties and performance of membranes. The structures and properties of membranes were characterized using atomic force microscopy (AFM), field-emission scanning electron microscopy, attenuated total reflectance-Fourier transform infrared spectroscopy (ATR-FTIR) and water contact angle measurements. The performance of the prepared membranes was evaluated by investigating the rejection capability of membranes towards $Cr(NO_3)_3$ and $Pb(NO_3)_2$ solutions. Fouling resistance of the prepared membranes was also studied.

2. Experimental setup

2.1. Materials

PES (58 kg/mol, Tg = 225°C) was obtained from BASF Company (Germany). N,N-dimethylforamide (DMF), polyvinylpyrrolidone (PVP, 25 kg/mol), were supplied from Merck (Germany). Thionyl chloride ($SOCl_2$) was distilled from boiled linseed oil prior to use. Triethylamine (Et_3N) was dried over calcium hydride (CaH_2) and then distilled. The bovine serum albumin (BSA) powder was obtained from Sigma. Monohydrate citric acid, tetrahydrofuran (THF), $Pb(NO_3)_2$ and $Cr(NO_3)_3$ standard reference materials were supplied from Merck (Germany).

2.2. Preparation of GO nanoparticles

GO nanoparticles were prepared from graphite according to Hummers method [3]. A schematic of the process of GO preparation is presented in Fig. 1.

2.3. Preparation of acyl-chloride-functionalized GO (GO-CO-Cl)

1 g GO powder was well dispersed by sonication for 1 h in 10 ml dry DMF. Then, 60 ml $SOCl_2$ (0.82 M) added at 80°C and the solution was refluxed for 3 d. The product was separated by centrifugation, then washed with anhydrous THF, and dried under vacuum [4].

2.4. Preparation of citric acid-decorated graphene oxide nanoparticle

Citric acid-decorated graphene oxide (GO-CA) was synthesized through the esterification reaction of GO-CO-Cl and CA [4]. First, 0.05 g GO-CO-Cl was dispersed in 30 ml dry THF under argon atmosphere. Afterwards, 3 g CA and 1 ml Et_3N were added into the solution at 0°C. The mixture was stirred for 1 h at 0°C, and was kept at room temperature for 6 h; then it was refluxed for 24 h. The powder was carefully washed with deionized water and ethanol. The resulting powder was dried under vacuum overnight (see Fig. 1).

2.5. Membrane preparation

Asymmetric PES membranes containing GO-CA nanoparticles were prepared via immersion phase inversion method using casting solutions containing PES, PVP (pore-forming

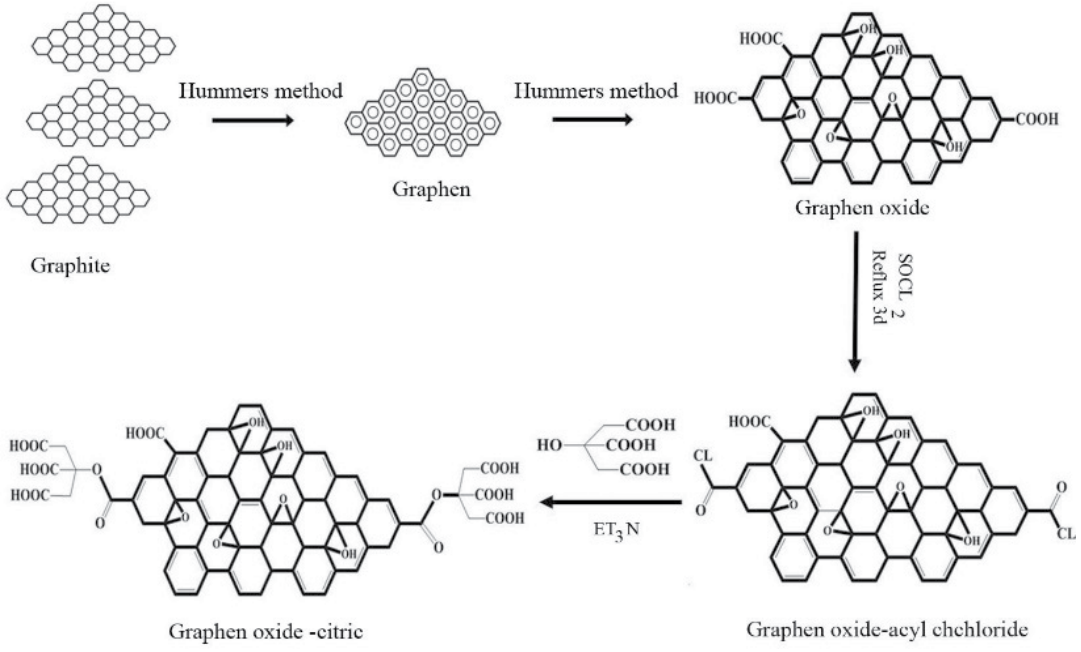

Fig. 1. Schematic of the preparation of GO and GO-CA.

agent) and different amounts of GO-CA nanoparticles (additive) in DMF. In brief, a certain amount of GO-CA nanoparticles was dispersed into DMF and sonicated for 30 min to obtain a homogenous dispersion. Then, PES and PVP were dissolved in the previously prepared solution and the consequent casting solution was stirred for 4 h at 50°C at 300 rpm. Dope solution was kept at ambient temperature for around 24 h to remove all air bubbles [5,6]. A sonication assisted method was used for further 10 min to obtain a homogeneous dispersion [1]. Afterwards, the prepared dope solution was cast on a clean glass plate with 250 μm thickness using a film applicator at room temperature without evaporation. Immediately after casting, glass plate was immersed into distilled water bath at room temperature. After primary phase separation and membrane formation, the membranes were immersed into distilled water for 24 h. Finally, membranes were dried for 24 h at room temperature [7]. The composition of casting solutions is tabulated in Table 1.

2.6. Characterization of GO and GO-CA nanoparticles and prepared membranes

Chemical and physical structures of GO and GO-CA were examined using Fourier-transform infrared spectroscopy (FTIR, Equniox 55 Brouker, Germany) and X-ray diffraction (XRD, Siemens, D5000, Germany) techniques. Also, to evaluate the existence of GO-CA, the prepared membranes were analyzed by (ATR-FTIR, Equniox 55 Brouker, Germany).

In addition, the morphology of the prepared membranes was evaluated by scanning electron microscopy (SEM) (Vega Tescan, Czech). Surface roughness and morphology of prepared membranes were investigated using AFM technique. Surface roughness parameters were reported in terms of average roughness (S_a), the root mean square of Z data (S_q) and mean difference between the highest peaks and lowest valleys (S_z).

2.7. Water uptake and contact angle measurement

Surface hydrophobicity/hydrophilicity of the membranes was examined by measuring the contact angle between membrane surface and water by sessile drop method. The contact angle was measured using a contact angle measuring instrument (G10, Kruss, Germany). Deionized water was used as probe liquid in all measurements. Contact angles for each membrane were measured at five random locations and their average value was reported to minimize experimental error [7]. The hydrophilic property of the prepared membranes was also studied by water uptake measurement. First, the membrane (1 cm^2) was immersed in demineralized water for 24 h and was weighed after drying with paper. Afterwards, the wet membrane was kept in a vacuum oven at 75°C for 24 h and the dried membrane was weighed. Water uptake was calculated using Eq. (1):

$$\text{water uptake (\%)} = \frac{\omega_s - \omega_d}{\omega_d} \times 100 \quad (1)$$

where ω_s (g) and ω_d (g) are the weights of wet and dry membranes, respectively [6].

Table 1
Composition of casting solution

Membrane	(wt.%)			
	GO-CA	PES	PVP	MDF
M_0	0.0	19	2	79
M_1	0.01	19	2	78.99
M_2	0.05	19	2	78.95
M_3	0.1	19	2	78.9

2.8. Porosity and pore size

The porosity (ε) of the prepared membranes was determined using gravimetric method. It was calculated using the following equation [8]:

$$\varepsilon = \frac{(\omega_1 - \omega_2)/d_\omega}{(\omega_1 - \omega_2/d\omega) + \omega_2/d_p} \quad (2)$$

where ω_1 is the weight of wet membrane (g), ω_2 is the weight of dry membrane (g), d_ω is pure water density (0.998 g/cm^3) and d_p is polymer density (1.43 g/cm^3).

To determine the mean pore radius (nm) of membrane, Guerout-Elford-Ferry equation [Eq. (3)] was employed which is calculated using pure water flux and porosity data [8].

$$r = \sqrt{\frac{(2.9 - 1.75\varepsilon) \times 8\eta l Q}{A \times \varepsilon \times \Delta P}} \quad (3)$$

where η is water viscosity (8.9 × 10^{-4} Pa s), l is membrane thickness (m), Q is permeation rate (m^3/s), A is the effective area of the membrane (m^2), and ΔP is trans-membrane pressure difference (0.6 M Pa).

2.9. Permeation and rejection tests

The performances of the prepared membranes were analyzed in terms of different factors including pure water flux and rejection of $Cr(NO_3)_3$ and $Pb(NO_3)_2$ solutions at pH = 2 (in order to stabilization of heavy metals in aqueous medium, the feed solution pH was adjusted at 2). These tests were performed using a dead-end filtration system. The effective area of membranes was nearly 12.56 cm^2 and its holder was connected to a nitrogen gas line. The permeate solution of each membrane was collected and weighed by an analytical balance. Initially, each membrane was compacted at 0.8 MPa with distilled water for 40 min. The operating pressure was adjusted at 0.6 MPa and then distilled water was passed through the membranes and permeance was weighed at 10 min intervals.

Pure water flux J_w (kg/m^2h) of each membrane was determined using the following equation:

$$J = \frac{M}{A\Delta t} \quad (4)$$

where M (kg) is the weight of permeated pure water, A (m^2) is membrane effective area, and Δt (h) is permeation time.

For the evaluation of performance, divalent and trivalent ion rejections were determined using 100 ppm $Cr(NO_3)_3$ and $Pb(NO_3)_2$ feed solutions at pH = 2 under pressure of 0.6 MPa. Then, for each membrane, the concentration of the collected permeate was measured using a conductivity meter (WTW COND 730 Model, Germany). The rejection of divalent and trivalent ions was obtained by Eq. (5):

$$R(\%) = \left[1 - \frac{\lambda_p}{\lambda_f}\right] \times 100 \tag{5}$$

where λ_p and λ_f versus μs/cm unit are ion conductivities in permeate and feed solutions, respectively.

2.10. Fouling tests

After measuring the pure water flux of each membrane, J_{wi} (kg/m^2 h), BSA solution (200 mg/L) was replaced in the stirred cell, and after 2 h filtration at 0.6 MPa, BSA solution flux was measured, J_p (kg/m^2 h). After the filtration of BSA solution, the fouled membrane in the dead-end cell was cleaned by filtration of distilled water for 15 min. Afterwards, distilled water was refilled into the cell and the pure water flux of cleaned membrane was measured again, J_{wc} (kg/m^2 h).

Finally, in order to determine the fouling resistant capability of the prepared membranes, flux recovery ratio (FRR) was calculated using Eq. (6):

$$\mathrm{FRR}(\%) = \left(\frac{J_{wc}}{J_{wi}}\right) \times 100 \tag{6}$$

Reversible fouling (R_r), irreversible fouling (R_{ir}) and total fouling (R_t) were calculated using Eqs. (7)–(9) [9]:

$$R_r(\%) = \left(\frac{J_{wc} - J_p}{J_{wi}}\right) \times 100 \tag{7}$$

$$R_{ir}(\%) = \left(\frac{J_{wi} - J_{wc}}{J_{wi}}\right) \times 100 \tag{8}$$

$$R_t(\%) = R_r(\%) + R_{ir}(\%) \tag{9}$$

3. Results and discussion

3.1. Characterization of GO and GO-CA nanoparticles and PES/GO-CA membranes

The FTIR spectra of GO and GO-CA are shown in Fig. 2a. The diagram of GO (Fig. 2Aa) shows one peak at 1,724 cm^{-1} which was attributed to C=O stretching vibration of –COOH group [1]. The bands at 1,216 and 1,037 cm^{-1} could be associated with C–O stretching vibrations of alkoxy, and this indicated that carboxylic acid groups were attached onto the surface of graphene [1,2]. The spectrum also showed two bands at 3,409 and 1,410 cm^{-1} which could be assigned to the stretching vibrations of O–H [1,10]. The FTIR spectrum of GO-CA, as can be seen in Fig. 2Ab, is differs from that of GO. The peak at 3,409 cm^{-1} on the diagram of GO was related to O–H (Fig. 2Aa). The peak broadness for GO-CA was reduced and shifted to 3,437 cm^{-1} (Fig. 2Ab) owing to the esterification of carboxylic acid groups of GO and the presence of aliphatic carboxylic acid groups of CA. Due to the esterification of carboxylic acid groups of GO, the peak at 1,724 cm^{-1} on the diagram of GO (Fig. 2Aa) was shifted to 1,737 cm^{-1} (Fig. 2Ab) [4].

As can be seen in Fig. 2Ab, new band at 2,923 cm^{-1} was attributed to CH_2 groups of CA [4]. Therefore, it could be confirmed that GO-CA was functionalized with CA. XRD patterns were used for further studying the changes in the structure of GO and GO-CA, and the results are shown in Fig. 2Ba. Usually, graphite (Fig. 2Ba) shows a very strong peak at $2\theta = 26.22°$, but oxidation generates oxygen-containing groups on graphite [4,10]. Therefore, GO (Fig. 2Ba) shows a very strong peak at $2\theta = 10.9°$ [10]. But, according to, the XRD patterns of GO-CA (Fig. 2Bb), the peak of CA-functionalized GO shifted back by around $2\theta = 25.84°$ which clearly confirmed the formation of GO-CA [4].

To investigate structural changes of membrane when GO-CA was used as an additive, ATR-FTIR was employed. Fig. 2C shows the ATR spectra of prepared membranes. Prepared membranes had similar spectral characteristics. The band at 1,667 cm^{-1} could be attributed to the carbonyl group of PVP [11]. In fact, this peak indicates that PVP was not completely leached out. However, PVP is a pore-forming and water-soluble agent which most of that is leached out during the phase inversion process, resulting in entrapping a little portion of PVP in the membrane matrix. [12].

The bands at 1,292 and 1,146 cm^{-1} were attributed to asymmetric and symmetric stretching of O=S=O groups of PES chains, respectively [2,10]. The peak at 3,416 cm^{-1} could be attributed to –OH stretching [6].

But, as displayed in Figs. 2Cb and c, when GO-CA content was increased (M_1 and M_2), peak intensity at 3,416 cm^{-1} was gradually increased compared with M_0 and M_3 (Figs. 2Ca and d). This means that hydroxyl and carboxyl functional groups were trapped on membrane surface.

But, as shown in Fig. 2Cd, in M_3, peak intensity at 3,416 and at 1,667 cm^{-1} was decreased in comparison with other membranes (Figs. 2Ca–c). As shown in Fig. 3, this might be due to hydrogen bonding interactions between $–SO_2$ groups of PES and carboxylic groups of GO-CA [13]. This means that hydroxyl functional groups were entrapped in membrane matrix, and the peak intensity at 3,416 cm^{-1} (attributed to –OH stretching) decreased (Fig. 2Cd). Researchers have found that the interactions between PES and PVP could be either between pyrrolidone groups in PVP and sulfone groups in PES or between side cyclic groups of PVP and aromatic ring of PES (π–π stacking interaction between GO-CA and PES) [11,14]. These interactions ensure that PVP molecules would be entrapped and remained in PES membrane matrix and surface, even after washing the PES membrane with large amount of water [11,14]. But it seems that higher GO-CA concentration (for M_3), due to the formation of a stronger hydrogen bonding (Fig. 3) interactions between $–SO_2$ groups of PES and carboxylic groups of GO-CA [13], the peak intensity at 1,667 cm^{-1} (attributed to the carbonyl group of PVP) decreased (Fig. 2Cd). This means that PVP molecules for M_3 are almost leached out from the membrane structure (Fig. 2Cd).

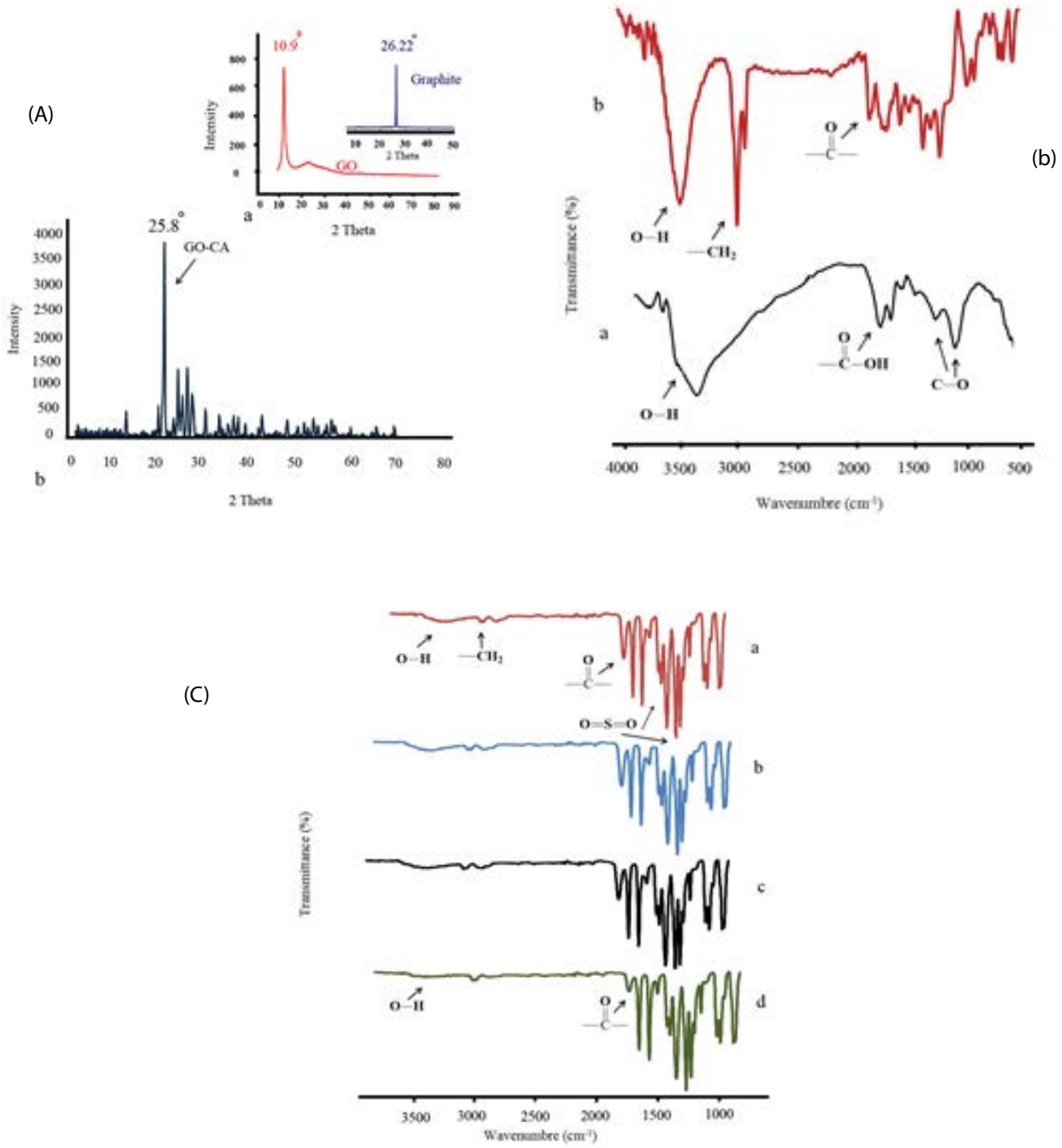

Fig. 2. (A) FTIR spectrum of (a) GO and (b) GO-CA, (B) Patterns XRD of (a) GO and graphite [10], (b) GO-CA and (C) FTIR-ATR spectra of (a) M_0, (b) M_1, (c) M_2 and (d) M_3 membranes.

3.2. Hydrophilicity evaluation of the prepared membranes

3.2.1. Contact angle

The water contact angles of prepared membranes are presented in Table 2. M_0 showed higher contact angle of about 67.7 ± 1.9. After loading GO-CA at 0.01 and 0.05 wt.%, water contact angle was reduced to 61.9 ± 2.8 and 61 ± 0.7, respectively.

Lower contact angle indicated more hydrophilicity of membrane surfaces. This could be due to the fact that hydrophilic nanoparticles spontaneously migrated towards the surface of the prepared membranes during phase inversion process [1].

Water contact angle of M_3 was 67.3 ± 2.2, which indicated that the hydrophilicity of the membrane was decreased with the increase of the amount of GO-CA in matrix polymer. As

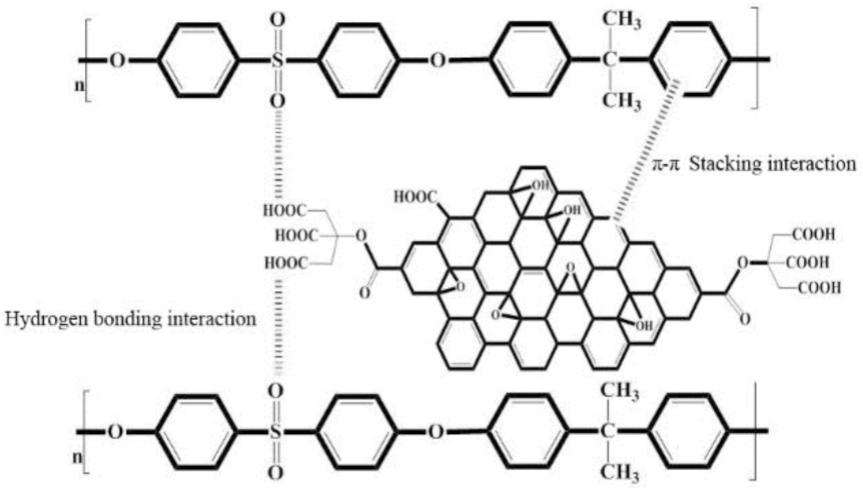

Fig. 3. Hydrogen bonding interactions between $–SO_2$ groups of PES and the –COOH groups of GO-CA in the modified membranes.

Table 2
Physico-chemical properties of the prepared membranes

Membranes	Water uptake (%)	Contact angle (°)	Porosity (%)	Average pore diameter (nm)	Zeta potential (mV)	Roughness parameters (nm)		
						S_z	S_a	S_q
M_0	66.4 ± 1.1	67.7 ± 1.9	80	1.7	–17.1	44.6	6.1	8.2
M_1	67.3 ± 0.8	61.9 ± 2.8	86	1.8	–14.6	25.1	3.8	4.0
M_2	71.5 ± 1	61.0 ± 0.7	89	1.9	–13.2	29.9	5.3	6.6
M_3	65.2 ± 1.9	67.3 ± 2.2	83	1.4	–4.1	25.2	3.2	4.1

seen in Fig. 3, this could be due to decreased effective surface area of nanoparticles at high blending ratios, due to entrapped GO-CA in membrane matrix via hydrogen bonding interactions between $–SO_2$ groups of PES and –COOH groups of GO-CA which led to the decrease of functional groups on membrane surface. This was also clearly demonstrated in the ATR-IR spectra of the membranes modified with 0.1 wt.% GO-CA where the peak intensity of –OH group (3,416 cm^{-1}) was decreased by the addition of additive (Fig. 2Cd).

3.2.2. Water uptake

Water uptake capacity of the prepared membranes mainly depend on two factors: (i) The presence of hydrophilic sites (–COOH and –OH) in membrane matrix and (ii) the morphology of the prepared membrane in terms of the presence of wider finger-like pores in membrane sub-layer [10]. The water uptake values of membranes are summarized in Table 2. The amount of water uptake capacity for M_2 was higher than other membranes (71.5%). This indicated that M_2 could absorb more water molecules due to higher number of hydrophilic sites on the surface of membrane. In fact, CA contains three ionizable hydrogen atoms which can have higher dipole interactions ($–COO^-$…H) with water molecules, leading to the creation of a water layer on the surface [6]. Also, it has been observed in SEM images (Fig. 4) that, the presence of GO-CA in casting solution created much wider finger-like pores in the sub-layer of M_1 and M_2 (Fig. 4b and c) than M_0 and M_3 (Fig. 4a and d) Consequently, water uptake capacities of M_1 and M_2 were higher than the other membranes.

3.3. Morphology of GO-CA embedded PES membranes

In order to study the influence of different concentrations of GO-CA nanoparticles on the structure and morphology of the prepared membranes, the surface and cross-section of membranes were observed using SEM. The cross-sectional SEM images of membranes with different concentrations of GO-CA are exhibited in Fig. 4. As shown in Fig. 4a–d, all prepared membranes exhibited asymmetric porous structures comprising a dense top-layer and a finger-like porous sublayer. Finger-like pores (Figs. 4b and c) in M_1 and M_2 were broader than that those in other membranes (Figs. 4a and d).

Fig. 5 shows the surface SEM images of prepared membranes. As can be seen, the surface of modified membranes was relatively smooth and glossy. In addition, no cracks were seen on the surface of modified membranes which illustrated that the membranes would not become friable and fragile in the presence of GO-CA [1]. It is worth mentionable that in several non-carbonic nanoparticles such as Fe_2O_3/SiO_2 [15] and TiO_2 [16] nanoparticles, the nanoparticles are

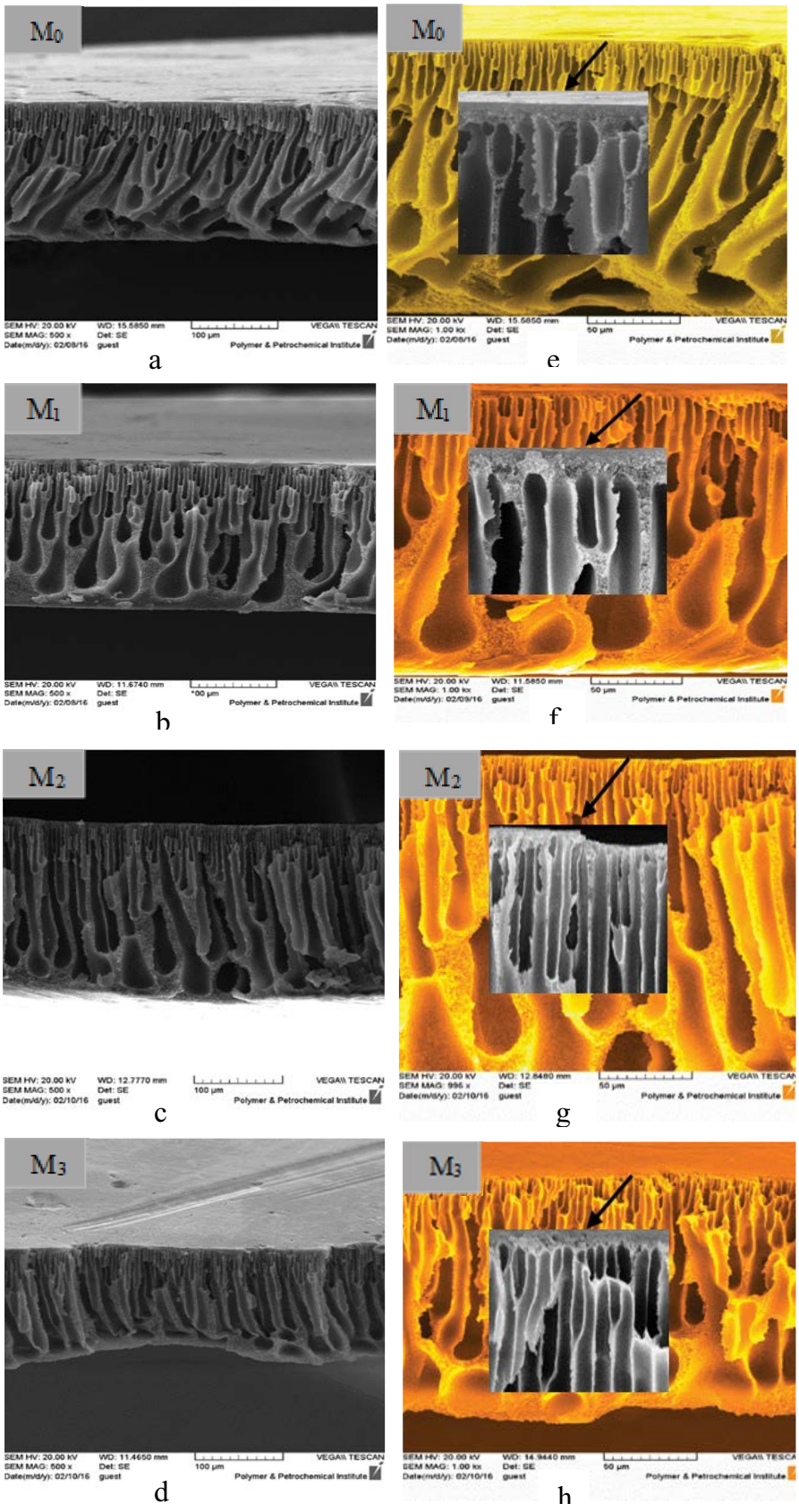

Fig. 4. Cross-sectional SEM images of membranes: (a) M_0, (b) M_1, (c) M_2, (d) M_3 and skin-layer thickness of the prepared membranes: (e) M_0, (f) M_1, (g) M_2 and (h) M_3.

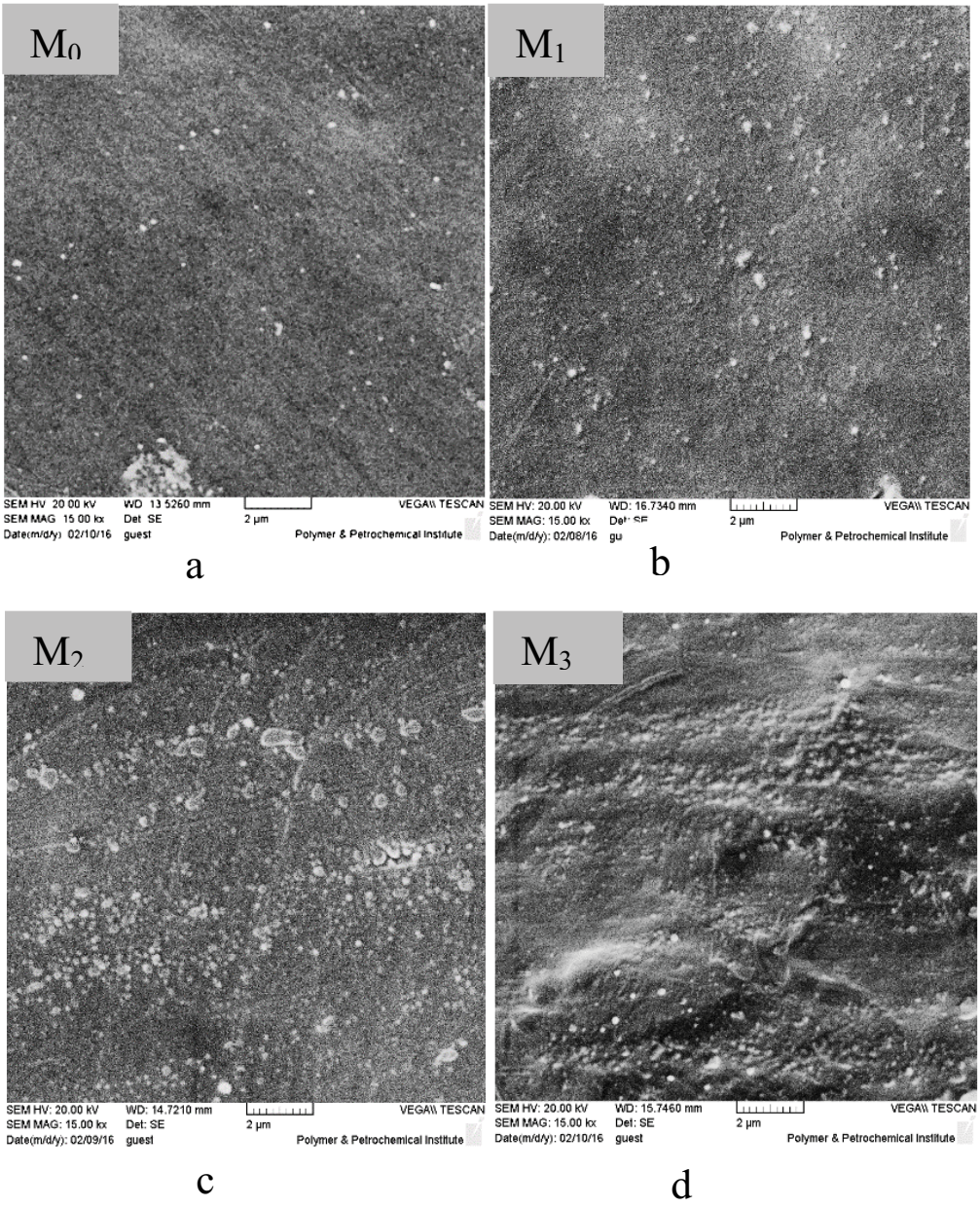

Fig. 5. Top surface SEM images of membranes: (a) M_0, (b) M_1, (c) M_2 and (d) M_3.

obviously observed in the membrane surface. However, in carbon-based nanoparticles such as carbon nanotube [17,18] and GO [1] nanoparticle on the surface was not observed.

Surface roughness of the prepared membranes was determined using AFM images and SPM software. Surface images of the prepared membranes are shown in Fig. 6. Surface roughness parameters of the prepared membranes are represented in Table 2.

As seen in Table 2, the surface roughness of the unmodified membrane was higher than those of modified membranes. By adding GO-CA into membrane matrix, membrane surfaces became smoother (Fig. 6b). This behavior was reported by Zinadini et al. [1] for GO/PES, Zhao et al. [19] for isocyanate-treated GO/PSF and Zhao et al. [20] for GO/PVDF membranes. In fact, at lower concentrations of GO-CA nanoparticle in M_1 (Fig. 6b), nanoparticles regularly collocated in membrane matrix owing to their low electrostatic interactions [1]. Consequently, the surface of M_1 became smoother (Fig. 6b).

M_2 showed more roughness than other modified membranes (Fig. 6c and Table 2). This could be due to the hydrophilic nature of GO-CA [10]. In general, the hydrophilic nature of GO-CA increased mass transfer rate between solvent and non-solvent during phase inversion and led to the formation of wider pore channels in sub-layer [18].

Fig. 6d indicates that the roughness of M_3 was reduced. This could be due to the increased viscosity of membrane casting solution, because increased viscosity reduced the

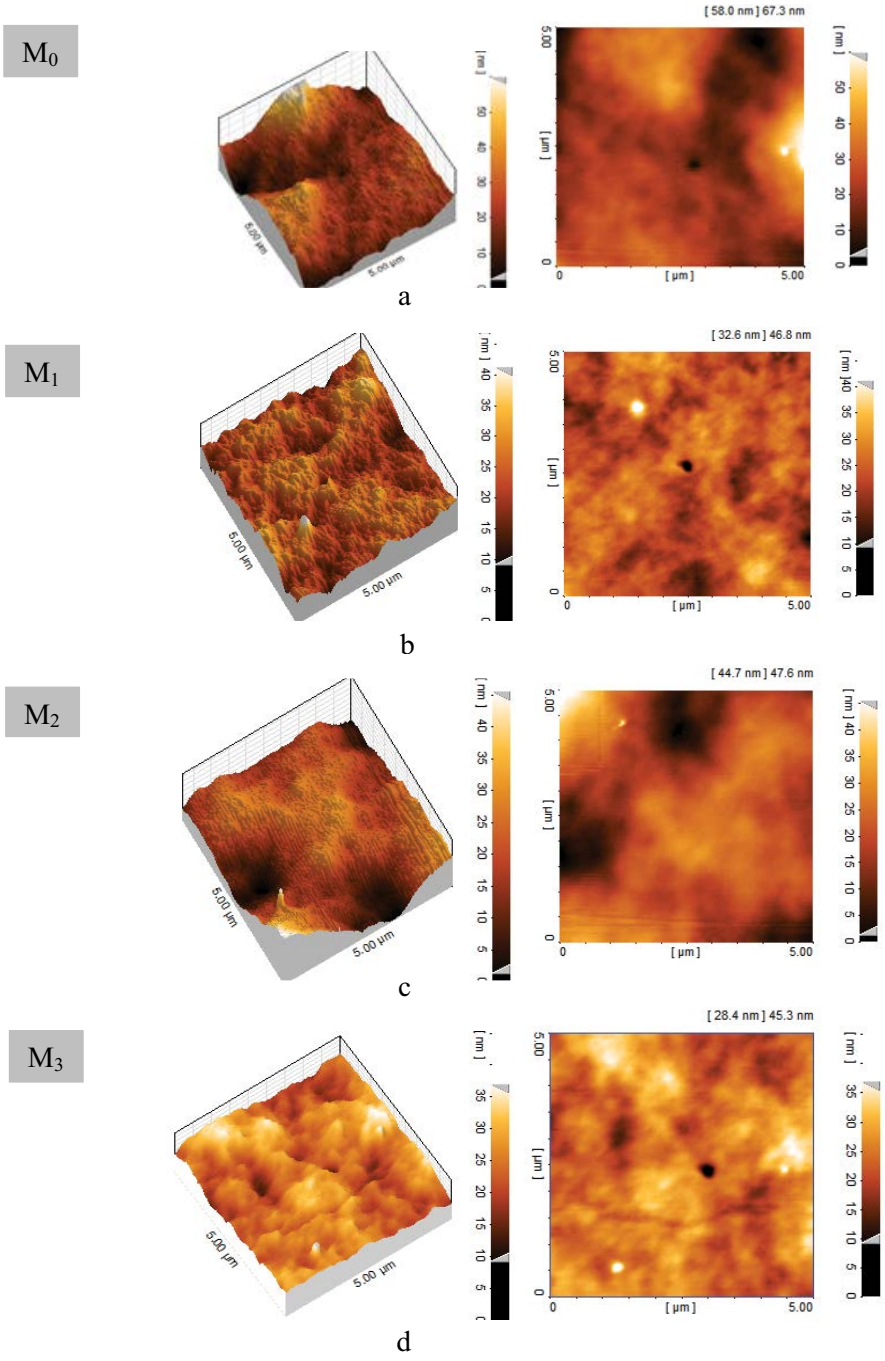

Fig. 6. AFM images of the PES membranes with different concentrations of the GO-CA: (a) M_0, (b) M_1, (c) M_2 and (d) M_3.

exchange of solvent and non-solvent, and accordingly membrane surface became smooth again [21].

The porosity and mean pore radius of the prepared membranes are presented in Table 2.

The porosity and mean pore radius of membranes were increased after loading GO-CA and reduced with addition of GO-CA in membrane matrix.

The porosity and mean pore radius of membranes were increased and then reduced with further addition of GO-CA in membrane matrix. This could be attributed to some factors such as changes in the amorphous nature of membranes, viscosity of casting solution and hydrophilic effect of GO-CA [1,21].

Usually, the membranes with high porosity are obtained from casting solutions with lower viscosity which causes faster exchange between solvent and non-solvent in the phase inversion process [21]. At low concentration of GO-CA nanoparticles in M_1 and M_2, the increase of GO-CA content, and therefore its hydrophilic effect, increased finger-like pore size, surface roughness, pore size and porosity of the

membranes [18,21]. But when the content of GO-CA was increased to 0.1 wt.%, as seen in Table 2, surface roughness, porosity and mean pore radius were decreased. This was probably due to the increase of the viscosity of membrane casting solution [17,18,21]. In fact, when the content of GO-CA was increased to 0.1 wt.%, the viscosity of casting solution became important, causing lower porosity due to the decrease of precipitation rate in phase inversion process. Although the viscosity was not measured accurately, the mentioned behavior has clearly been explained in literature [17,18,21]. Alterations in porosity is in consistency with increasing mean pore radius, water uptake and contact angle of the prepared membranes (Table 2).

3.4. Membrane performance evaluation

Generally, two major factors influenced membrane performance, hydrophilicity and morphology: (i) the increases of flux due to enhancing the hydrophilicity of the modified membranes and (ii) the decrease of flux due to reduced membrane pore size, porosity and increase thicker skin layer [22].

Fig. 7 clearly shows the effect of GO-CA on the water flux of the prepared membranes. As it can be seen, the water flux of the modified membranes was enhanced when the loading amount of GO-CA in the matrix of membrane was increased to 0.01 and 0.05 wt.% and then decreased with further increase of the loading amount of GO-CA to 0.1 wt.%.

Therefore, the trend of increasing water flux would be explained in hydrophilicity changes (due to water uptake and contact angle), increasing pore radius and porosity of the membranes (Table 2). The results summarized in Table 2 indicated that modified membranes with a little larger pores were formed by the addition of 0.01 and 0.05 wt.% GO-CA into casting solution. Thus, the water flux of M_1 and M_2 was increased (Fig. 7). However, the water flux of M_3 was decreased to 12.8 kg/m²h. The results summarized in Table 2 show that mean pore radius of the surface, water uptake and porosity of M_3 decreased, resulted in decreasing water flux (Fig. 7).

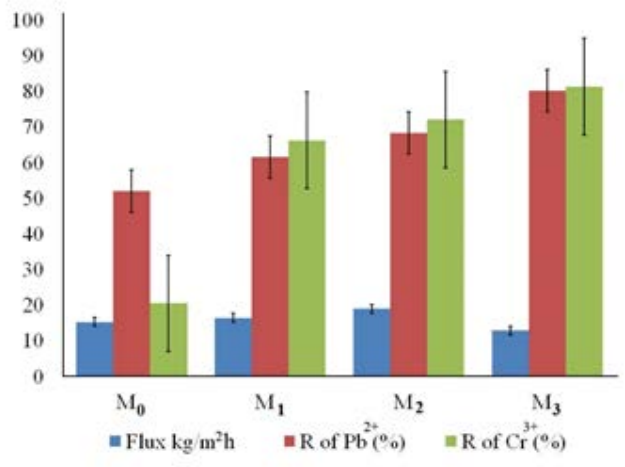

Fig. 7. Water flux and rejection (*R*) capability of the membranes against Pb and Cr ions.

Based on SEM images (Fig. 4), the changes induced in the skin layer of the prepared membranes were evaluated. Thicker and denser skin layer (Fig. 4e) of M_0 as well as its lower porosity and water uptake (Table 2) reduced its pure water flux (Fig. 7). Decreased thickness (Fig. 4f), sponge-like structures, high porosity (Table 2) and water uptake of skin layer of M_1 increased water flux.

As shown in Fig. 4g, significant decrease in top-layer thickness was clearly observed by the addition of GO-CA in M_2. Thus, significant reduction in the thickness of skin layer, increase porosity and water uptake (Table 2) of M_2 increased water flux. The thickness of skin layer of M_3 was increased (Fig. 4h) that could be explained by either changing of the viscosity of casting solution by the addition of nanoparticles at high percentages. Consequently, due to Fig. 4h thicker skin layer with lower porosity and water uptake (Table 2) showed less flux [2].

Fig. 7 shows the effect of different concentrations of GO-CA on the rejection of $Cr(NO3)_3$ and $Pb(NO3)_2$ solutions at pH = 2. As seen in Fig. 7, by increasing GO-CA content in matrix polymer, rejection capability of the modified membranes was increased. The rejection capability of the M_3 membrane was higher than that of other membranes. As seen in Table 2, smaller pore radius of M_3 increased the rejection capability of the membrane. In spite of increasing mean pore radius of M_1 and M_2, the rejection capability of the membranes was increased (Fig. 7). Generally, the charge of the membrane and the valence of the ions can influence the rejection of ions [23]. As seen in Fig. 8a, a hydration layer was formed on the surface of the modified membranes at pH = 2 via electrostatic and hydrogen bonding interactions [21]; thus, the modified membranes had positive outer surface charge at the studied pH, and this caused high rejection between positive ions and positive surface charges of the modified membranes.

The surface charges of the prepared membranes were measured with zeta potential under tangential flow mode and presented in Table 2. Zeta potential values were negative for all prepared membranes at pH = 5.4 and were decreased with increasing the amount of GO-CA in membrane matrix. This was because CA in GO-CA nanomaterial contained three carboxylic acid functional groups, and they easily interacted with hydronium ion at pH = 5.4 and therefore, a hydration layer was formed on the surface of the modified membranes making their zeta potential values less negative.

Zeta potential values on M_0 were –17.1 mV. The rejection of the negatively charged membrane was:

$$\%\ R\ (Pb(NO_3)_2) > \%\ R\ (Cr(NO_3)_3) \quad (10)$$

On the other hand, zeta potential values were less negative for modified membrane, but in all modified membranes, the rejection of Cr^{3+} was higher than Pb^{2+}. As explained above, modified membranes had positively charged outer surfaces at pH = 2. Therefore, they had higher retention values for trivalent Cr^{3+} ion than bivalent Pb^{2+} ion [24]. Consequently, Donnan exclusion played a vital role in the ion rejection of the modified membranes.

Fouling is the most detrimental disadvantage of membrane technology which hampered the beneficial use of membranes, because foulants could be absorbed into the

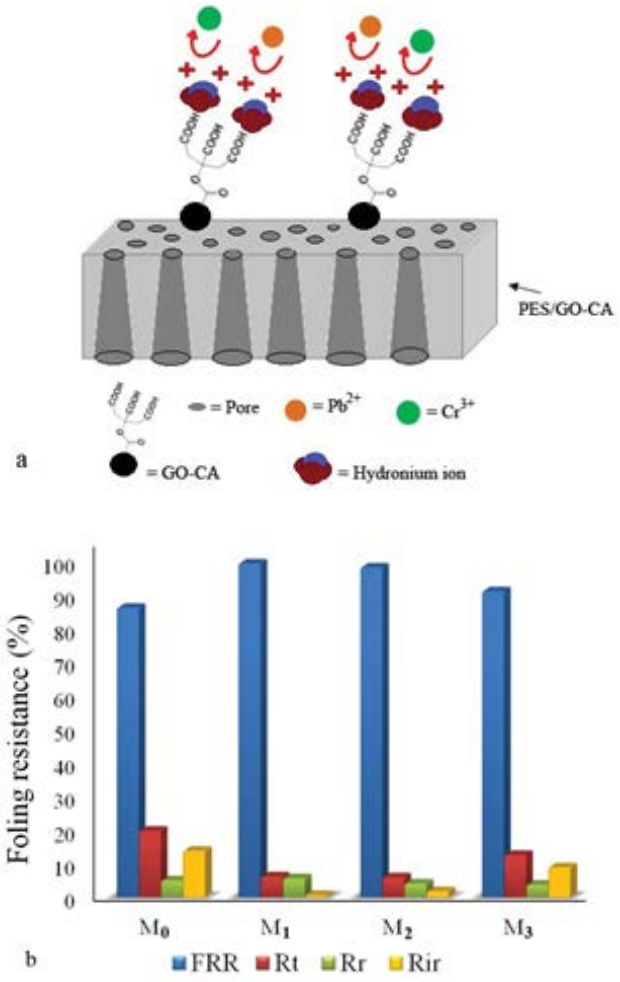

Fig. 8. (a) Schematic representation of formation a hydration layer on the surface of modified membranes at pH = 2 and (b) antifouling properties of the prepared membranes.

pores on membrane surface resulting in the clogging of pores reducing the yield and lifetime of membrane.

The anti-fouling performance of prepared membranes was determined by measuring their water flux recovery after BSA solution filtration. The FRR of the prepared membranes are presented in Fig. 8b. Higher FRR indicates better anti-fouling feature of the prepared membranes. FRR of M_0 (86.2 %) was lower than those of modified membranes and signified poor anti-fouling property of M_0. The best FRR value was obtained for M_1 (99.4%). This indicated that the modified membranes had high anti-fouling property. Several parameters could influence the anti-fouling properties of membranes such as hydrophilicity, surface roughness and charge. M_0 with the highest roughness and lowest hydrophilicity had lowest FRR value. FRR of M_2 was lower than that of M_1, while the contact angle of M_2 (61°) was lower than that of M_1 (61.9°), probably due to the increase of surface roughness of M_2 (Table 2), because the low contact angle of M_2, did not significantly increase its hydrophilicity. FRR of M_3 (91.1%) with the lower roughness was lower than that of other modified membranes probably due to lower hydrophilicity of M_3 (Table 2).

The isoelectric point of BSA molecules is about 4.9 [6], and the pH value of BSA solution was 7. Under this condition, BSA molecules were negatively charged. On the other hand, the CA of the additive GO-CA, is a poly-carboxylic acid and contains three ionizable hydrogen atoms. It can easily be ionized at pH = 7. In fact, three carboxylic acid functional groups induce negative charge on modified membrane surfaces at pH = 7. Consequently, the electrostatic repulsion of negatively charged BSA molecules and modified membrane surfaces was an important reason for improving the anti-fouling performance of the membranes prepared in this study [6].

R_t, R_r and R_{ir} values of the prepared membranes are represented in Fig. 8b. The obtained results exhibited that the resistance factors of the modified membranes were lower than that of the pristine one, while their FRR was higher. The total fouling resistance of the modified membranes, which is the sum of R_r and R_{ir}, was considerably lower than that of unmodified membrane. The R_{ir} of the membranes was considerably reduced from 13.8% for unmodified membrane to 0.6% for M_1. In summary, FRR, R_r, and R_{ir} of the modified membranes were improvement. These results indicated that modified membranes had significant anti-fouling properties.

4. Conclusions

In this work, GO-CA was firstly synthesized and then the effect of GO-CA nanocomposite on the morphology and performance of polyethersulphone membranes was evaluated. The results obtained for the performance of the prepared membranes showed that loading GO-CA into membrane matrices increased their pure water flux and heavy metals ion rejection. The results confirmed that strong electrostatic repulsion forces between ions and membrane surfaces played an important role in the ion rejection of the modified membranes at acidic pHs. In fact, Donnan exclusion was the dominant mechanism in ion rejection. Water uptake capacity, water contact angle and surface free energy values confirmed the enhanced hydrophilicity of M_1 and M_2 comprising appropriate nanosheets loads. The hydrophilic nature of GO-CA led to the establishment of wider finger-like pores in sub-layer, and made membrane surfaces smoother in comparison with M_0. The surface porosity and mean pore radius of M_1 and M_2 were enhanced with the increase of GO-CA. The results of anti-fouling experiments illustrated that the hydrophilicity and surface roughness of the prepared membranes played a vital role in the anti-fouling resistance of PES/GO-CA membranes, and M_1, with low roughness and high hydrophilicity, had the best anti-fouling properties. The results also showed that the FRR of the modified membranes was meaningfully increased.

References

[1] S. Zinadini, A.A. Zinatizadeh, M. Rahimi, V. Vatanpour, H. Zangeneh, Preparation of a novel antifouling mixed matrix PES membrane by embedding graphene oxide nanoplates, J. Membr. Sci., 453 (2014) 292–301.

[2] N. Meng, Z.Y. Wang, Z.-X. Low, Y.Q. Zhang, H.T. Wang, X.W. Zhang, Impact of trace graphene oxide in coagulation bath on morphology and performance of polysulfone ultrafiltration membrane, Sep. Purif. Technol., 147 (2015) 364–371.
[3] W.S. Hummers Jr., R.E. Offeman, Preparation of graphitic oxide, J. Am. Chem. Soc., 80 (1958) 1339–1339.
[4] M. Namvari, H. Namazi, Synthesis of magnetic citric-acid-functionalized graphene oxide and its application in the removal of methylene blue from contaminated water, Polym. Int., 63 (2014) 1881–1888.
[5] Y. Mansourpanah, S.S. Madaeni, A. Rahimpour, Z. Kheirollahi, M. Adeli, Changing the performance and morphology of polyethersulfone/polyimide blend nanofiltration membranes using trimethylamine, Desalination, 256 (2010) 101–107.
[6] R.S. Hebbar, A.M. Isloor, A.F. Ismail, S.J. Shilton, A. Obaid, H.-K. Fun, Probing the morphology and anti-organic fouling behaviour of a polyetherimide membrane modified with hydrophilic organic acids as additives, New J. Chem., 39 (2015) 6141–6150.
[7] Y. Mansourpanah, S.S. Madaeni, A. Rahimpour, M. Adeli, M.Y. Hashemi, M.R. Moradian, Fabrication new PES-based mixed matrix nanocomposite membranes using polycaprolactone modified carbon nanotubes as the additive: property changes and morphological studies, Desalination, 277 (2011) 171–177.
[8] N.A.A. Hamid, A.F. Ismail, T. Matsuura, A.W. Zularisam, W.J. Lau, E. Yuliwati, M.S. Abdullah, Morphological and separation performance study of polysulfone/titanium dioxide (PSF/TiO_2) ultrafiltration membranes for humic acid removal, Desalination, 273 (2011) 85–92.
[9] Y. Mansourpanah, S.S. Madaeni, A. Rahimpour, A. Farhadian, A.H. Taheri, Formation of appropriate sites on nanofiltration membrane surface for binding TiO_2 photo-catalyst: Performance, characterization and fouling-resistant capability, J. Membr. Sci., 330 (2009) 297–306.
[10] B.M. Ganesh, A.M. Isloor, A.F. Ismail, Enhanced hydrophilicity and salt rejection study of graphene oxide-polysulfone mixed matrix membrane, Desalination, 313 (2013) 199–207.
[11] B. Vatsha, J.C. Ngila, R.M. Moutloali, Preparation of antifouling polyvinylpyrrolidone (PVP 40K) modified polyethersulfone (PES) ultrafiltration (UF) membrane for water purification, Phys. Chem. Earth., 67–69 (2014) 25–131.
[12] M. Sun, Y. Su, C. Mu, Z. Jiang, Improved antifouling property of PES ultrafiltration membranes using additive of silica-PVP nanocomposite, Ind. Eng. Chem. Res., 49 (2010) 790–796.
[13] E. Celik, H. Park, H. Choi, H. Choi, Carbon nanotube blended polyethersulfone membranes for fouling control in water treatment, Water Res., 45 (2011) 274–282.
[14] L.Y. Lafreniere, F.D.F. Talbot, T. Matsuura, S. Sourirajan, Effect of poly(vinylpyrrolidone) additive on the performance of poly(ether sulfone) ultrafiltration membranes, Ind. Eng. Chem. Res., 26 (1987) 2385–2389.
[15] Y. Mansourpanah, A. Rahimpour, M. Tabatabaei, L. Bennett, Self-antifouling properties of magnetic Fe_2O_3/SiO_2-modified poly (piperazine amide) active layer for desalting of water: characterization and performance, Desalination, 419 (2017) 79–87.
[16] A. Rahimpour, S.S. Madaeni, A.H. Taheri, Y. Mansourpanah, Coupling TiO_2 nanoparticles with UV irradiation for modification of polyethersulfone ultrafiltration membranes, J. Membr. Sci., 313 (2008) 158–169.
[17] J.-H. Choi, J. Jegal, W.-N. Kim, Fabrication and characterization of multi-walled carbon nanotubes/polymer blend membranes, J. Membr. Sci., 284 (2006) 406–415.
[18] V. Vatanpour, S.S. Madaeni, R. Moradian, S. Zinadini, B. Astinchap, Fabrication and characterization of novel antifouling nanofiltration membrane prepared from oxidized multiwalled carbon nanotube/polyethersulfone nanocomposite, J. Membr. Sci., 375 (2011) 284–294.
[19] H. Zhao, L. Wu, Z. Zhou, L. Zhang, H. Chen, Improving the antifouling property of polysulfone ultrafiltration membrane by incorporation of isocyanate-treated graphene oxide, Phys. Chem. Chem. Phys., 15 (2013) 9084–9092.
[20] C. Zhao, X. Xu, J. Chen, F. Yang, Effect of graphene oxide concentration on the morphologies and antifouling properties of PVDF ultrafiltration membranes, J. Environ. Chem. Eng., 1 (2013) 349–354.
[21] M. Kumar, M. Ulbricht, Novel antifouling positively charged hybrid ultrafiltration membranes for protein separation based on blends of carboxylated carbon nanotubes and aminated poly(arylene ether sulfone), J. Membr. Sci., 448 (2013) 62–73.
[22] A. Rahimpour, M. Jahanshahi, S. Khalili, A. Mollahosseini, A. Zirepour, B. Rajaeian, Novel functionalized carbon nanotubes for improving the surface properties and performance of polyethersulfone (PES) membrane, Desalination, 286 (2012) 99–107.
[23] M. Nilsson, G. Trägårdh, K. Östergren, The influence of pH, salt and temperature on nanofiltration performance, J. Membr. Sci., 312 (2008) 97–106.
[24] J.M.M. Peeters, J.P. Boom, M.H.V. Mulder, H. Strathmann, Retention measurements of nanofiltration membranes with electrolyte solutions, J. Membr. Sci., 145 (1998) 199–209.